

# A Quasi-Multinary Composite Coating on a Nickel-Rich NCM Cathode Material for All-Solid-State Batteries

David Kitsche,<sup>[a]</sup> Florian Strauss,\*<sup>[a]</sup> Yushu Tang,<sup>[b]</sup> Nikolai Bartnick,<sup>[a]</sup> A-Young Kim,<sup>[a]</sup> Yuan Ma,<sup>[a]</sup> Christian Kübel,<sup>[b, c, d, e]</sup> Jürgen Janek,<sup>[a, f]</sup> and Torsten Brezesinski\*<sup>[a]</sup>

Inorganic solid-state batteries are attracting significant interest as a contender to conventional liquid electrolyte-based lithium-ion batteries but still suffer from several limitations. The search for advanced coatings for protecting cathode materials in solid-state batteries to achieve interfacial stability is a continuing challenge. In the present work, the surface of an industrially relevant Ni-rich  $\text{LiNi}_x\text{Co}_y\text{Mn}_z\text{O}_2$  cathode material, NCM-851005 (85 % Ni), was modified by applying a coating containing Li, Nb and Zn, aiming at a composition  $\text{Li}_6\text{ZnNb}_4\text{O}_{14}$ , by means of sol-gel chemistry. Detailed characterization using scanning trans-

mission electron microscopy combined with energy-dispersive X-ray spectroscopy and nano-beam electron diffraction showed that the surface layer after heating in  $\text{O}_2$  at 500 °C contains  $\text{Li}_3\text{NbO}_4$  nanocrystals and  $\text{Li}_2\text{CO}_3$ , with Zn presumably acting as a dopant. The protective coating on the NCM-851005 secondary particles significantly increased the cycling performance (reversible capacity, rate capability etc.) and stability of full cells using argyrodite  $\text{Li}_6\text{PS}_5\text{Cl}$  as solid electrolyte. Interestingly, the level of improvement is superior to that achieved with conventional  $\text{LiNbO}_3$  coatings.

## Introduction

Engineering of stable interfaces is one of the major challenges on the route to bulk-type solid-state batteries (SSBs) that are capable of competing with liquid electrolyte-based Li-ion batteries (LIBs) in terms of electrochemical performance.<sup>[1–3]</sup> Lithium thiophosphates, which exhibit the highest room-temperature ionic conductivities<sup>[4]</sup> among the reported superionic solid electrolytes (SEs) along with favorable mechanical

properties, have been shown to be unstable when in contact with energy-dense cathode active materials (CAMs), such as  $\text{LiNi}_x\text{Co}_y\text{Mn}_z\text{O}_2$  (referred to as NCM), especially at the high voltages they are usually operated at.<sup>[5–11]</sup> Therefore, it is imperative to introduce a buffer layer between CAM and SE. In the past, various protective CAM coatings prepared by different techniques have been reported.<sup>[12–18]</sup> Wet-chemical methods have been applied most often because of their simplicity, low costs and good scalability.<sup>[12]</sup> Despite numerous reports on the beneficial effects of CAM coatings, such as reduced interfacial resistance and improved cycling stability, the quest for new materials or improving on established ones is ongoing. Specific chemical compositions and structures have been targeted to attain desired functionalities, typically based on the bulk properties of the respective materials. However, it has been shown that the microstructure and coating composition can deviate strongly from the bulk, especially if sol-gel methods are used in the preparation.

Ternary lithium niobium oxides, often assumed to be present as  $\text{LiNbO}_3$ , are among the best-performing coating materials and have been studied in considerable detail.<sup>[12–15]</sup> The relatively high room-temperature ionic conductivity in the amorphous state is regarded as one of the reasons for the suitability of  $\text{LiNbO}_3$  in the SSB field.<sup>[19]</sup> Because of difficulties in characterizing nanoscale coatings on CAMs, their microstructure and chemical identity are often not examined in detail. However, in a recent study, the sol-gel derived Li–Nb–O-type coating has been shown to be particulate in nature, with  $\text{LiNbO}_3$  nanoparticles surrounded by a  $\text{Li}_2\text{CO}_3$ -containing shell.<sup>[14]</sup>

In this work, we focus on a compound of composition  $\text{Li}_6\text{ZnNb}_4\text{O}_{14}$ , referred to as LZNO. This particular material has previously been investigated as a potential SE.<sup>[20,21]</sup> The metastable oxide was found to undergo disproportionation

[a] D. Kitsche, Dr. F. Strauss, N. Bartnick, Dr. A-Y. Kim, Dr. Y. Ma, Prof. J. Janek, Dr. T. Brezesinski  
Battery and Electrochemistry Laboratory, Institute of Nanotechnology, Karlsruhe Institute of Technology (KIT), Hermann-von-Helmholtz-Platz 1, 76344 Eggenstein-Leopoldshafen, Germany  
E-mail: florian.strauss@kit.edu  
torsten.brezesinski@kit.edu

[b] Dr. Y. Tang, Prof. C. Kübel  
Institute of Nanotechnology, Karlsruhe Institute of Technology (KIT), Hermann-von-Helmholtz-Platz 1, 76344 Eggenstein-Leopoldshafen, Germany

[c] Prof. C. Kübel  
Karlsruhe Nano Micro Facility (KNMF), Karlsruhe Institute of Technology (KIT), Hermann-von-Helmholtz-Platz 1, 76344 Eggenstein-Leopoldshafen, Germany

[d] Prof. C. Kübel  
Helmholtz Institute Ulm (HIU), Helmholtzstr. 11, 89081 Ulm, Germany

[e] Prof. C. Kübel  
Technical University Darmstadt, Department of Materials and Earth Sciences, Alarich-Weiss-Str. 2, 64287 Darmstadt, Germany

[f] Prof. J. Janek  
Institute of Physical Chemistry & Center for Materials Research (ZfM/LaMa), Justus-Liebig-University Giessen, Heinrich-Buff-Ring 17, 35392 Giessen, Germany

 Supporting information for this article is available on the WWW under <https://doi.org/10.1002/batt.202100397>

 © 2022 The Authors. *Batteries & Supercaps* published by Wiley-VCH GmbH. This is an open access article under the terms of the Creative Commons Attribution License, which permits use, distribution and reproduction in any medium, provided the original work is properly cited.

into  $\text{Li}_3\text{NbO}_4$ ,  $\text{Li}_{1-x}\text{NbO}_3$  and  $\text{LiZnNbO}_4$  upon cooling after high-temperature solid-state synthesis. Nonetheless, the conductivity of the as-obtained composite material was relatively high, approximately  $3 \times 10^{-5}$  S/cm at room temperature, making the Li–Zn–Nb–O system attractive for CAM coatings. Here, we surface-modified a Ni-rich NCM CAM,  $\text{LiNi}_{0.85}\text{Co}_{0.10}\text{Mn}_{0.05}\text{O}_2$  (NCM-851005), aiming at the nominal coating composition of LZNO, for application in lithium thiophosphate-based SSB cells.

## Results and Discussion

The NCM-851005 CAM was first heated in  $\text{O}_2$  at  $750^\circ\text{C}$  to reduce the amount of surface impurities, followed by coating using a sol-gel route, similar to recent studies.<sup>[15,22,23]</sup> The treated material was then heated in  $\text{O}_2$  at 100, 300 or  $500^\circ\text{C}$ . The respective samples are referred to as LZNONCM-100/300/500 hereafter. Using inductively coupled plasma-optical emission spectroscopy (ICP-OES), the Zn and Nb weight fractions were determined to be 0.077(1) and 0.50(1) wt.%, respectively, slightly below the targeted values of 0.093 and 0.53 wt.% (corresponding to 1 wt.% LZNO). Note that the molar ratio of  $n(\text{Nb}):n(\text{Zn}) \approx 4.57$  also deviated from the stoichiometric ratio of 4.

Figure 1(a-d) shows low- and high-magnification scanning electron microscopy (SEM) images of the bare NCM-851005 and LZNO-NCM-500 (LZNO-NCM-100/300 are shown for com-

parison in Figure S1, Supporting Information). The morphology of the base CAM was found to remain unaltered upon coating. However, small amounts of agglomerated coating material were observed to be randomly distributed over the secondary particles, as somewhat expected for a non-optimized sol-gel synthesis. These observations were made irrespective of the heating temperature.

The presence of  $\text{Li}_2\text{CO}_3$  in the bare and coated NCM-851005 CAMs was verified via attenuated total reflection-infrared (ATR-IR) spectroscopy (Figure S2, Supporting Information), with minor differences between the spectra. This result indicates that some surface impurities from the synthesis remained, and the carbonate content did not change much with coating. According to elemental analysis, the  $\text{Li}_2\text{CO}_3$  content was approximately 0.5 wt.% in all samples. Note that previous studies have demonstrated that carbonate species, as part of hybrid or solid-solution coatings, can be beneficial to the SSB performance.<sup>[15,24]</sup>

X-ray diffraction (XRD) was used to assess possible changes in lattice structure of the coated samples. All reflections in the patterns of the different CAMs can be indexed within the  $R\text{-}3m$  space group ( $\alpha\text{-NaFeO}_2$ -type structure), as expected for NCM materials (Figure 2). In addition, refinement analysis (see Figure S3, Supporting Information, for Rietveld profiles) revealed that the crystal structure remains largely unaffected (Table 1).

Based on electrochemical performance screening of the coated NCM-851005 CAMs (Figure S4, Supporting Information),

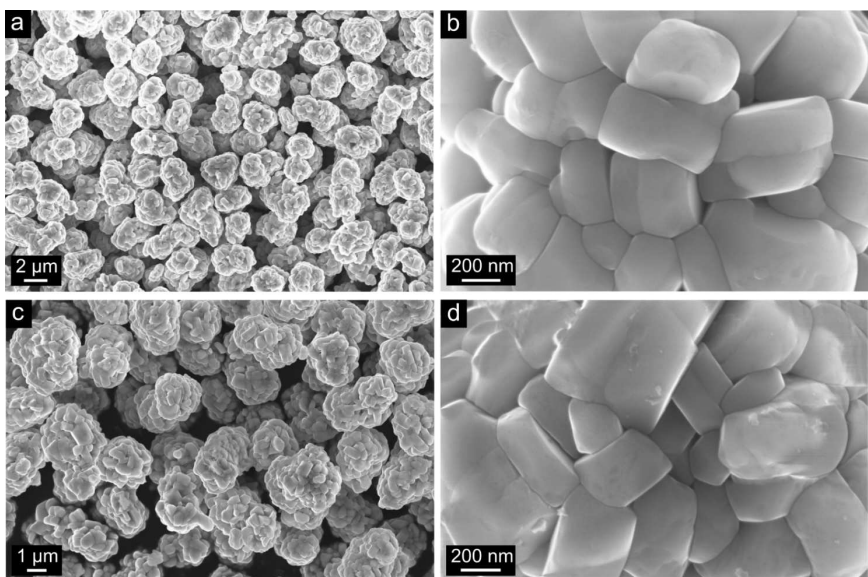
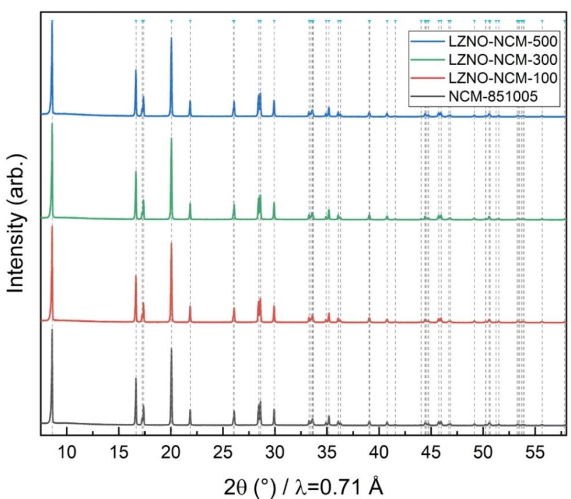


Figure 1. SEM images at different magnifications of a, b) bare NCM-851005 and c, d) LZNO-NCM-500.

**Table 1.** Refined structural parameters of bare and LZNO-coated NCM-851005 CAMs.

Sample	Rf [%]	$a$ [ $\text{\AA}$ ]	$c$ [ $\text{\AA}$ ]	$V$ [ $\text{\AA}^3$ ]	$z$ of O	$u_{\text{iso}}$ Li site [ $\text{\AA}^2$ ]	$u_{\text{iso}}$ TM site [ $\text{\AA}^2$ ]	Ni on Li site
NCM-851005	2.07	2.86993(7)	14.1872(3)	101.197(4)	0.2420(2)	0.018(2)	0.0052(2)	0.027(2)
LZNO-NCM-100	1.97	2.87017(7)	14.1866(3)	101.211(4)	0.2421(1)	0.021(2)	0.00500(2)	0.031(2)
LZNO-NCM-300	1.58	2.87028(6)	14.1858(3)	101.213(3)	0.2419(1)	0.025(2)	0.0032(2)	0.036(2)
LZNO-NCM-500	2.4	2.87048(7)	14.1869(3)	101.234(4)	0.2419(2)	0.021(2)	0.0054(2)	0.032(2)



**Figure 2.** Normalized XRD patterns collected from bare and LZNO-coated NCM-851005 CAMs.

LZNO-NCM-500 was selected for more detailed investigations. Transmission electron microscopy (TEM) was used to gain insights into the microstructure of the coating. The presence of an amorphous shell on the secondary particles was evidenced by high-resolution TEM (Figure S5, Supporting Information). Figure 3(a) presents a low-magnification high-angle annular dark-field scanning TEM (HAADF STEM) image, showing the coating on the outer surface of a focused ion beam (FIB)-prepared NCM-851005 particle cross-section. The thickness of this layer ranged from a few nanometers to a few tens of nanometers, and the coating appeared to be somewhat thicker at the outward facing grain boundaries (see also Figure S6, Supporting Information). The presence of uncoated (free) surfaces is in principle conceivable but was not apparent from the imaging data.

The chemical composition of the coating was further probed using energy-dispersive X-ray spectroscopy (EDS). Figure 3(b) shows a higher magnification HAADF STEM image and corresponding elemental maps of the surface region of a FIB-prepared particle cross-section. A clear separation of CAM and coating was evident in STEM dark-field mode, coinciding with the locations of Ni and Nb. Diffusion of Nb into the bulk was not observed, in agreement with expectations considering the size and charge of the Nb ions. The elemental map of Zn suggests its presence both in the coating and in the NCM-851005 CAM. However, given the minor Zn content, the EDS results are not unambiguous. This issue was not to be solved by electron energy-loss spectroscopy (EELS) either because of overlap of the Ni L-edge (1008 eV) and Zn L-edge (1020 eV) and the very low amount of Zn relative to that of Ni. Hence, elucidating the specific role of Zn in the LZNO-NCM requires further study.

Crystalline species in the amorphous surface layer were detected by nano-beam electron diffraction (NBED; Figure S7, Supporting Information). Virtual dark-field images (see Figure S8, Supporting Information, for details on the 4D-STEM approach) revealed the presence of nanoparticles (Figure 3c,

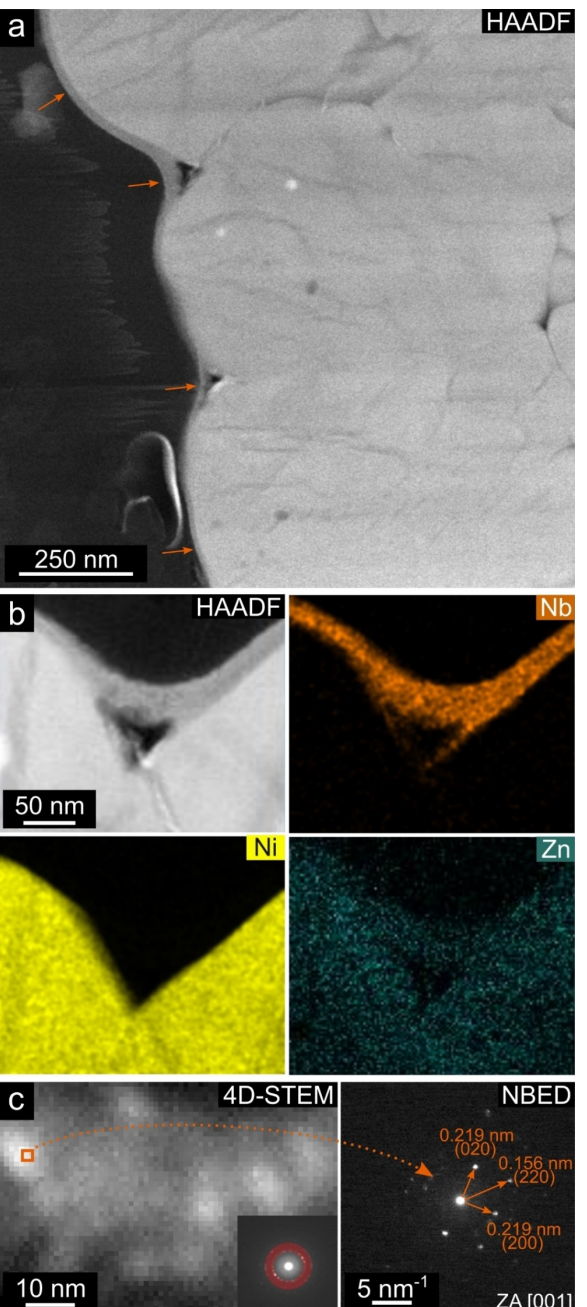


**Figure 3.** Electron microscopy of LZNO-NCM-500. a) Low-magnification HAADF STEM image of a FIB-prepared particle cross-section, with orange arrows indicating the coating. b) High-magnification HAADF STEM image and corresponding elemental maps. c) Left: Virtual dark-field image (aperture indicated in the inset diffraction pattern) of the coating from a 4D-STEM dataset. Right: Indexed NBED pattern of the area denoted on the left.

left side) having a cubic crystal structure (Figure 3c, right side), unlike the targeted monoclinic LZNO.<sup>[20]</sup> Previous studies have shown that the latter phase can only be obtained at high temperatures and is not stable upon cooling. However, a room-temperature ionic conductivity of  $\sigma_{Li} \approx 3 \times 10^{-5}$  S/cm has been reported for the resulting composite material, which is in the range of that of good oxide Li-ion conductors.<sup>[21]</sup> The lattice spacings match well with those of rocksalt-type (*Fm-3m* space

group) lithium niobium oxides, such as  $\text{Li}_3\text{NbO}_4$  and related compounds.<sup>[25,26]</sup> Note that cubic  $\text{Li}_3\text{NbO}_4$  has previously been prepared by a sol-gel method.<sup>[27]</sup> In addition, a broad reflection observed at low diffraction angles (see Figure S7, Supporting Information), not indexable in the  $Fm\text{-}3m$  space group, is probably resulting from partially crystalline  $\text{Li}_2\text{CO}_3$ , as observed by ATR-IR (Figure S2, Supporting Information). The protective surface layer thus shows similarities to previously reported  $\text{Li}_2\text{CO}_3/\text{LiNbO}_3$  hybrid coatings on an NCM-622 (60% Ni) CAM, where the lithium niobate was embedded in an amorphous carbonate matrix.<sup>[14,15,28]</sup>

Until recently, the presence of crystalline  $\text{Li}_3\text{NbO}_4$  in sol-gel derived Li–Nb–O-type coatings had not been demonstrated. This could be because the preparation conditions usually involve heating at temperatures below the onset of crystallization. Another reason could be the lack of advanced characterization techniques required to detect these species. Specifically, Nb coatings on NCM-811 (80% Ni) have been examined for their crystalline components.<sup>[29,30]</sup> In the first study,  $\text{LiNbO}_3$  and  $\text{Li}_3\text{NbO}_4$  have been predominantly observed at temperatures ranging from 400 to 500 °C and 700 to 800 °C, respectively (without comments on the lattice structures).<sup>[29]</sup> In the second study, the authors pointed out that  $\text{Li}_3\text{NbO}_4$  is much more abundant than  $\text{LiNbO}_3$  in the surface layer at 475 °C already but difficult to detect because of its low crystallinity.<sup>[30]</sup> Based on these results, we decided to probe a (bulk) mixture of the coating reagents in the absence of the NCM-851005 CAM *in situ* during heating in O<sub>2</sub> using XRD. The crystallization (onset) temperature was found to be approximately 470 °C (see contour plot in Figure S9, Supporting Information). The main component was  $\text{LiNbO}_3$  ( $R\bar{3}c$  space group).  $\text{Li}_3\text{NbO}_4$  identified via NBED could not be observed clearly by XRD, thereby indicating a different crystallization and/or phase formation behavior relative to the nanoscale coating on the surface of the layered oxide CAM. Regardless, the degree of crystallinity is assumed to be relevant, as the positive effect of lithium niobate coatings has been attributed in part to their favorable electrical transport properties. Apart from that, the identification of cubic  $\text{Li}_3\text{NbO}_4$ , which has recently received attention as a host structure for disordered rocksalt (DRX) CAMs,<sup>[31,32]</sup> expands the current perspective on Li–Nb–O-type protective coatings. Although  $\text{Li}_3\text{NbO}_4$  is an insulator, transition metal substitution can affect the cation ordering and result in a percolating network for lithium migration.<sup>[32]</sup> This could potentially be a new approach for the development of advanced coating materials for SSB and/or LIB applications.

The electrochemical performance of the bare and coated NCM-851005 CAMs was probed at 45 °C in the voltage range 1.35–2.75 V vs.  $\text{Li}_4\text{Ti}_5\text{O}_{12}/\text{Li}_7\text{Ti}_5\text{O}_{12}$  (approximately 2.9–4.3 V vs. Li<sup>+</sup>/Li) in pellet-stack SSBs with argyrodite  $\text{Li}_6\text{PS}_5\text{Cl}$  (LPSCl) SE, used in the electrodes and separator, and with  $\text{Li}_4\text{Ti}_5\text{O}_{12}$  (LTO) as anode active material. LTO was chosen because of its zero-strain nature and favorable operating voltage range (note that the focus of the present work is on the NCM-851005 CAM). In fact, preliminary data confirm that the anode has no major effect on the cycling performance of the cathode. Figure 4(a) shows the first-cycle charge/discharge curves of representative

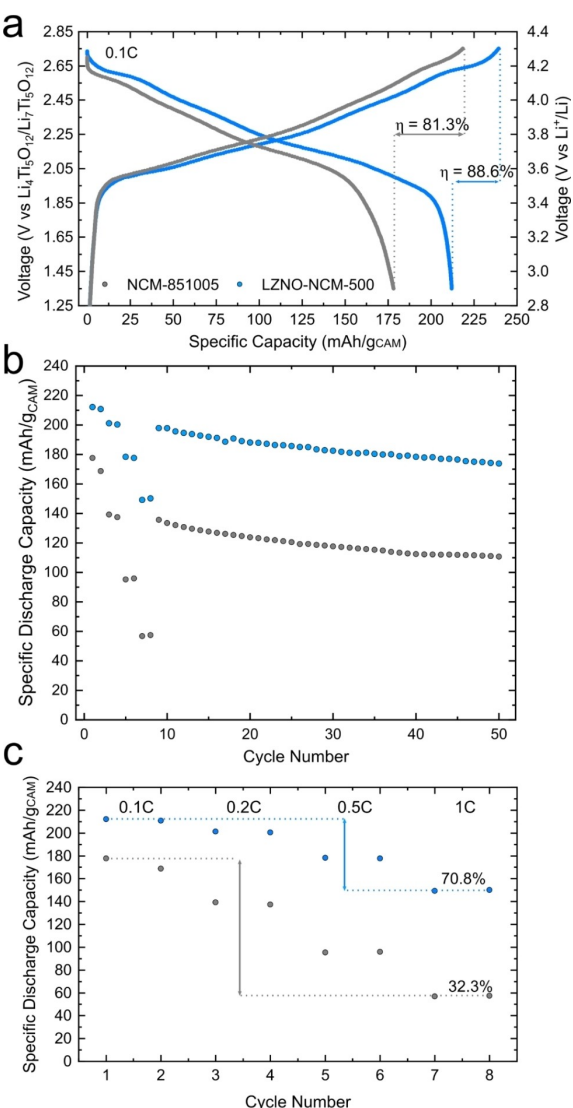


**Figure 4.** Electrochemical performance of bare NCM-851005 and LZNO-NCM-500 at 45 °C in pellet-stack SSB cells with an LTO anode and LPSCl as SE. a) First-cycle voltage profiles at 0.1 C and corresponding Coulombic efficiencies. b, c) Specific discharge capacities during rate capability testing, with two cycles each at 0.1 C, 0.2 C, 0.5 C and 1 C, followed by 0.2 C cycling. The percentage values in c) reflect the capacity retention at 1 C (8<sup>th</sup> cycle) relative to the first cycle at 0.1 C rate.

cells at a rate of 0.1 C. The LZNO-NCM-500 delivered a specific discharge capacity of 212 mAh/g<sub>CAM</sub> (approximately 2.2 mAh/cm<sup>2</sup>), compared to 178 mAh/g<sub>CAM</sub> for the bare NCM-851005, enabled by superior kinetics and reversibility. The voltage profile suggests improved delithiation, resulting in a larger capacity than for the uncoated counterpart. The difference in Coulombic efficiency, 88.6% vs 81.3% for the coated and uncoated CAM, respectively, indicates that more severe side reactions occurred in the case of bare NCM-851005.<sup>[14]</sup> This result helps to explain the strongly reduced overpotential observed for the LZNO-NCM-500. It should be noted that resistance buildup has been reported to result from detrimental chemical and electrochemical reactions between the electrode constituents during cycling operation, among others.

Interfacial degradation in lithium thiophosphate-based SSBs has already been studied in detail using X-ray photoelectron spectroscopy (XPS) and time-of-flight secondary ion mass spectrometry (ToF-SIMS), for example. SE oxidation, evident from the appearance of polysulfide and oxygenated sulfur/phosphorus species, typically occurs at the contact points between the particles upon charging, with the degree of interfacial degradation being significantly different for coated and uncoated CAMs.<sup>[5–8,14,18,24,33,34]</sup> The same is to be expected here. However, from the available literature reports, it is apparent that there are no clear trends of what coating chemistry and/or morphology works best in terms of suppressing the formation of certain degradation products.

Figure 4(b, c) shows the specific discharge capacities for rates between 0.1 C and 1 C. The overall performance of the LZNO-NCM-500 was clearly better than that of the uncoated CAM, with differences in capacity ranging from 30 to 90 mAh/g<sub>CAM</sub>. At 1 C (2 mA/cm<sup>2</sup>), a specific discharge capacity of approximately 150 mAh/g<sub>CAM</sub> was achieved with the LZNO-NCM-500, corresponding to 71% of the capacity at 0.1 C rate. In contrast, the bare NCM-851005 delivered a specific discharge capacity of approximately 57 mAh/g<sub>CAM</sub>, corresponding to only 32% of the initial capacity. These results emphasize the improved charge-transfer kinetics through the modified CAM|SE interface. The large cell capacities afforded by the coated CAM were also reasonably stable with  $q_{\text{dis}} \approx 174$  mAh/g<sub>CAM</sub> at 0.2 C in the 50<sup>th</sup> cycle.

Furthermore, the cyclability of the LZNO-coated NCM-851005 CAMs in SSB cells was evaluated against that of three analogously prepared reference coatings (Figure S10, Supporting Information). These coatings had nominal  $n(\text{Li}):n(\text{Nb})$  ratios of 1:1 (representing the LiNbO<sub>3</sub> stoichiometry), 1.5:1 (equal to LZNO but without Zn) and 3:1 (for Li<sub>3</sub>NbO<sub>4</sub>). As expected, all of them resulted in substantial improvements in cycling performance over the bare NCM-851005. Notably, the LZNO coating clearly outperformed the other Li–Nb–O-type protective coatings. Although the role of Zn is still largely unclear, its presence in the surface layer has a strong positive effect on the reversible capacity, rate capability and stability of the Ni-rich NCM CAM in SSBs with argyrodite Li<sub>6</sub>PS<sub>5</sub>Cl as SE. Because superior performance was also seen for the LZNO-NCM-300, the presence of crystalline components in the coating appears to play no major role though.

The long-term cycling stability of the two CAMs was also tested at 1 C (Figure 5a). As expected from the rate performance data shown in Figure 4(c), the LZNO-NCM-500 delivered superior specific capacities. While the bare NCM-851005 showed rapid capacity fading over the first 20 cycles, the capacity degradation of the LZNO-NCM-500 was found to occur more gradually. More than 81% of the initial discharge capacity was retained after 200 cycles, compared to only 68% for SSBs using the uncoated CAM, despite the much larger cumulative charge exchanged in the cells with the LZNO-NCM-500. Figure 5(b) shows the Coulombic efficiencies up to the 50<sup>th</sup> cycle. The LZNO-NCM-500 exhibited higher values throughout, with the differences being particularly significant over the first 20 cycles. This suggests faster formation of stable interfaces in

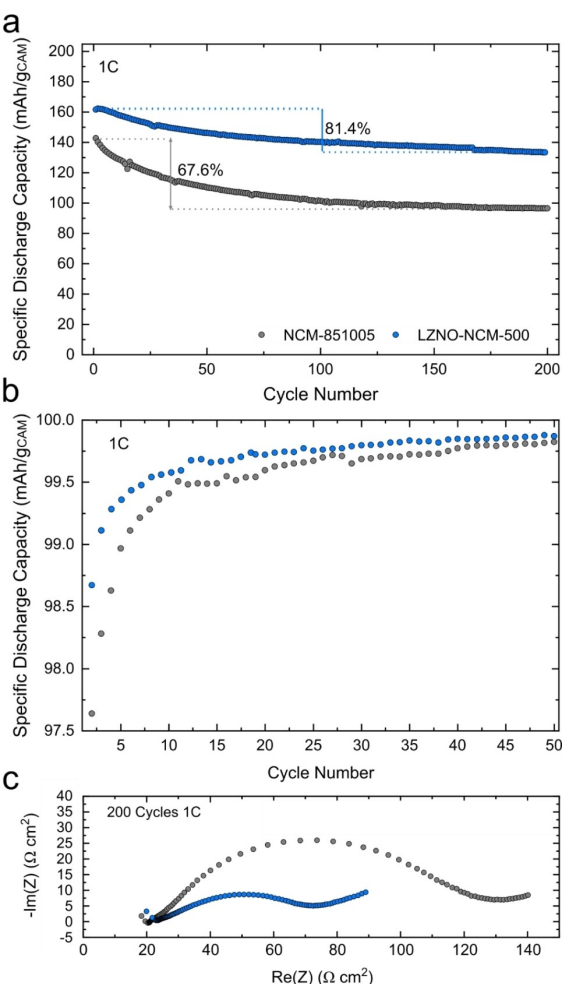


**Figure 5.** Electrochemical performance of bare NCM-851005 and LZNO-NCM-500 at 45 °C in pellet-stack SSB cells with an LTO anode and LPSCl as SE. a) Long-term cycling at 1 C rate. The percentage values indicate the capacity retention after 200 cycles. b) Corresponding Coulombic efficiencies from the 2<sup>nd</sup> cycle onward. c) Nyquist plots of the electrochemical impedance at 45 °C of representative cells after 200 cycles.

the case of coated CAM. Nonetheless, the Coulombic efficiencies converged during the course of cycling and stabilized above 99.9% after 60 cycles.

Finally, the SSBs after 200 cycles were examined by electrochemical impedance spectroscopy (EIS) and SEM. Figure 5(c) shows Nyquist plots from EIS measurements conducted on the cells using the bare and coated NCM-851005 in the discharged state. Semi-quantitative comparison of the depressed semi-circles representing the interfacial cathode resistance indicated that this contribution is reduced by a factor of about two with the LZNO-NCM-500 CAM. This finding corroborates the differences in Coulombic efficiency discussed above.

Figure S11 (Supporting Information) shows cross-sectional SEM images at different magnifications of cathodes harvested from the cycled cells. In both cases, there were no signs of major (chemo)mechanical degradation (contact loss, particle fracture etc.), implying that the differences in cycling performance between bare NCM-851005 and LZNO-NCM-500 mainly

arise from a different degree of (electro)chemical decomposition at the CAM|SE interface.

## Conclusion

In conclusion, application of a facile wet chemistry-based synthesis route led to the formation of a promising composite coating, containing  $\text{Li}_3\text{NbO}_4$  (or related) nanocrystals and  $\text{Li}_2\text{CO}_3$ , on a Ni-rich NCM cathode active material. Although the targeted phase  $\text{Li}_6\text{ZnNb}_4\text{O}_{14}$  could not be stabilized, the presence of rocksalt-type  $\text{Li}_3\text{NbO}_4$  expands the current perspective on Li–Nb–O derived protective coatings. The latter have thus far been present mostly in the form of (amorphous)  $\text{LiNbO}_3$ . Ultimately, the reported coating has proven to be highly beneficial to the cycling performance of argyrodite  $\text{Li}_6\text{PS}_5\text{Cl}$ -based solid-state battery cells, resulting in large capacities, high-rate capability and good capacity retention, and further shown to outperform conventional lithium niobate coating materials.

## Experimental Section

### Materials

$\text{LiNi}_{0.85}\text{Co}_{0.10}\text{Mn}_{0.05}\text{O}_2$  (NCM-851005,  $d_{50}=3.52\text{ }\mu\text{m}$ ,  $d_{90}=5.05\text{ }\mu\text{m}$ ; BASF SE) CAM was heated in  $\text{O}_2$  at  $750^\circ\text{C}$  for 3 h ( $5^\circ\text{C}/\text{min}$  heating rate) to reduce the amount of residual surface carbonates. 1 M lithium ethoxide solution was prepared by the reaction of absolute ethanol (Sigma-Aldrich; 99.8%) with Li metal (Albemarle Germany GmbH). To prepare 0.5 M niobium ethoxide and 0.01 M zinc acetate solutions,  $\text{Nb}(\text{OCH}_2\text{CH}_3)_5$  (Sigma-Aldrich; 99.95%) or  $\text{Zn}(\text{O}_2\text{CCH}_3)_2$  (Sigma-Aldrich) was dissolved in absolute ethanol.

### Surface coating

For the preparation of LZNO-coated NCM-851005 (with a nominal coating content of 1 wt.%), the CAM powder (5.94 g) was added to a mixture of lithium ethoxide (512  $\mu\text{L}$ ), niobium ethoxide (683  $\mu\text{L}$ ) and zinc acetate (8500  $\mu\text{L}$ ) solutions in an Ar-filled glovebox, followed by 30 min ultrasonication of the dispersion. Subsequently, the reaction mixture was dried in a vacuum overnight. The resultant powder was ground using a mortar and pestle and heated in  $\text{O}_2$  at 100, 300 or  $500^\circ\text{C}$  for 2 h ( $5^\circ\text{C}/\text{min}$  heating rate).

### Electrode preparation, cell assembly and testing

Cathode composite was prepared by mixing the bare or coated NCM-851005,  $\text{Li}_6\text{PS}_5\text{Cl}$  (LPSCl; NEI Corp.) and Super C65 carbon black (Timcal) in a ratio of 70:30:1 by weight in a planetary mill (Fritsch) at 140 rpm for 30 min. Using the same procedure, anode composite was prepared from carbon-coated  $\text{Li}_4\text{Ti}_5\text{O}_{12}$  (LTO; NEI Corp.), LPSCl and Super C65 at a weight ratio of 30:60:10 (30:65:5 in Figure 5).

The electrochemical performance of the bare and coated NCM-851005 was tested in SSB cells using a custom-built setup comprising a polyether ether ketone sleeve and two stainless steel dies. 10 mm diameter pellet stacks were prepared starting from the separator layer, made by cold pressing 100 mg LPSCl at a uniaxial pressure of 62 MPa. They were finished by adding 65 mg anode

composite and 12 mg cathode composite (approximately 2.9 mAh/cm<sup>2</sup>,  $q_{\text{th}}=274\text{ mAh/g}_{\text{CAM}}$ ) and pressing the stack at 437 MPa. All cells were galvanostatically cycled at  $45^\circ\text{C}$  in the voltage range 1.35–2.75 V vs.  $\text{Li}_4\text{Ti}_5\text{O}_{12}/\text{Li}_7\text{Ti}_5\text{O}_{12}$  (approximately 2.9–4.3 V vs.  $\text{Li}^+/\text{Li}$ ) while maintaining a uniaxial pressure of 81 MPa. Rate performance and stability tests were carried out at 0.1 C, 0.2 C, 0.5 C and 1 C, with two cycles at each rate, followed by further cycling at 0.2 C. Stability tests were performed at a rate of 1 C (1 C = 190 mA/g<sub>CAM</sub>) for 200 cycles.

### Methods

For compositional analysis, the LZNO-coated NCM-851005 was dissolved in acid using a graphite furnace. The Zn and Nb contents were determined by ICP-OES using a Thermo Fisher Scientific iCAP 7600 DUO. The C content was probed using a CS analyzer. Mass fractions represent the mean of at least three independent measurements.

SEM analysis was carried out at an accelerating voltage of 10 kV using a LEO-1530 electron microscope (Carl Zeiss AG) with a field emission source. Cross-sectional SEM images were taken from fractured electrode pellets after cycling.

ATR-IR spectroscopy was carried out using an ALPHA FT-IR spectrometer (Bruker), equipped with a Ge crystal.

TEM characterization was done using a double aberration corrected Themis-Z microscope (ThermoFisher Scientific) at an accelerating voltage of 300 kV, equipped with an OneView IS camera (AMETEK), a Super-X EDX detector (ThermoFisher Scientific) and a high-resolution GIF Continuum 970 (AMETEK) electron energy-loss spectrometer. 4D-STEM datasets were collected using the OneView IS camera with a screen current of approximately 10 pA, a small convergence semi-angle of 0.47 mrad and a camera length of 580 mm. Virtual imaging of the NBED patterns was done using DigitalMicrograph (version 3.42). Sample cross-sections were prepared using a dual-beam Ga FIB in a Strata 400 (ThermoFisher Scientific). Carbon layers were deposited by ion beam-induced deposition to protect the coating during sample preparation and processing. Initial thinning was performed at 30 kV. Final sample thinning and cleaning was done at 5 and 2 kV, respectively.

XRD patterns were collected from the samples using a Stadi-P diffractometer (STOE) with a Mo anode ( $\lambda=0.70926\text{ \AA}$ ) and a MYTHEN 1 K strip detector (DECTRIS AG) in Debye-Scherrer geometry. The instrumental contribution to the reflection broadening was obtained by measuring a NIST 640f Si standard reference material. Rietveld refinement was performed using GSAS-II.<sup>[35]</sup> During refinement, the scale factor, zero shift and crystallite size broadening parameters were allowed to vary. Sample absorption was calculated based on the capillary diameter of 0.3 mm and a powder packing density of 1.44 g/cm<sup>3</sup>. A Chebyshev polynomial function with 17 terms was used to fit a fixed background to the data. Unit cell parameters, oxygen site position and atomic displacement parameters (isotropic,  $u_{\text{iso}}$ ) for each site were refined. Atoms occupying the same site were constrained to have the same atomic parameters. Site occupancy factors were constrained such that each site remained fully occupied.

*In situ* heating XRD of a volume mixture of the LZNO coating was performed using a diffractometer equipped with a microfocus Mo  $K_{\alpha 1,2}$  rotating anode and a Pilatus 300 K-W area detector.<sup>[36]</sup> The precursor material was prepared by combining the Li, Nb and Zn solutions, followed by 30 min ultrasonication and solvent evaporation, as described above. It was packed into a sapphire capillary and heated at  $1^\circ\text{C}/\text{min}$  under  $\text{O}_2$  flow in a custom-built gas-flow furnace based on the design of Chupas *et al.* while recording XRD

patterns every 10 min.<sup>[37]</sup> Temperature calibration was carried out using the unit-cell volume evolution of an Al<sub>2</sub>O<sub>3</sub> reference material during application of the same heating profile.<sup>[38]</sup>

EIS was conducted on SSB cells after 200 cycles at frequencies from 7 MHz to 100 mHz (10 mV amplitude) using an SP-300 impedance analyzer (Bio-Logic Science Instruments Ltd.).

## Acknowledgements

This study was supported by BASF SE. The authors acknowledge the support from the Karlsruhe Nano Micro Facility (KNMF, www.knmf.kit.edu), a Helmholtz research infrastructure at Karlsruhe Institute of Technology (KIT, www.kit.edu). D.K. and F.S. acknowledge the Fonds der Chemischen Industrie (FCI) for financial support through Kekulé and Liebig fellowships. Y.T. acknowledges the financial support from the German Research Foundation (DFG) under project ID 390874152 (POLiS Cluster of Excellence). The authors thank Dr. Damian Goonetilleke (INT, KIT) for help with the Rietveld refinement analysis, Dr. Thomas Bergfeldt (IAM-AWP, KIT) for ICP-OES measurements, as well as Leonhard Karger (INT, KIT) and Dr. Holger Geßwein (IAM-ESS, KIT) for assistance with the *in situ* XRD experiment. They also thank Dr. Jörn Kulisch (BASF SE, Ludwigshafen) and Dr. Pascal Hartmann (BASF SE, Ludwigshafen) for fruitful discussions. Open Access funding enabled and organized by Projekt DEAL.

## Conflict of Interest

The authors declare no conflict of interest.

## Data Availability Statement

The data that support the findings of this study are available from the corresponding author upon reasonable request.

**Keywords:** all-solid-state battery • lithium nickel cobalt manganese oxide cathode • lithium niobate • lithium thiophosphate solid electrolyte • sol-gel coating

- [1] J. Janek, W. G. Zeier, *Nat. Energy* **2016**, *1*, 16141.
- [2] Y.-K. Sun, *ACS Energy Lett.* **2020**, *5*, 3221–3223.
- [3] S. Randau, D. A. Weber, O. Kötz, R. Koerver, P. Braun, A. Weber, E. Ivers-Tiffée, T. Adermann, J. Kulisch, W. G. Zeier, F. H. Richter, J. Janek, *Nat. Energy* **2020**, *5*, 259–270.
- [4] Y. Kato, S. Hori, T. Saito, K. Suzuki, M. Hirayama, A. Mitsui, M. Yonemura, H. Iba, R. Kanno, *Nat. Energy* **2016**, *1*, 16030.
- [5] A. Banerjee, X. Wang, C. Fang, E. A. Wu, Y. S. Meng, *Chem. Rev.* **2020**, *120*, 6878–6933.
- [6] J. Auvergniot, A. Cassel, J.-B. Ledeuil, V. Viallet, V. Seznec, R. Dedryvère, *Chem. Mater.* **2017**, *29*, 3883–3890.
- [7] S. Sun, C.-Z. Zhao, H. Yuan, Y. Lu, J.-K. Hu, J.-Q. Huang, Q. Zhang, *Mater. Futures* **2022**, *1*, 012101.
- [8] F. Walther, R. Koerver, T. Fuchs, S. Ohno, J. Sann, M. Rohnke, W. G. Zeier, J. Janek, *Chem. Mater.* **2019**, *31*, 3745–3755.
- [9] F. Strauss, D. Kitsche, Y. Ma, J. H. Teo, D. Goonetilleke, J. Janek, M. Bianchini, T. Brezesinski, *Adv. Energy Sustain. Res.* **2021**, *2*, 2100004.
- [10] K. J. Kim, M. Balaish, M. Wadaguchi, L. Kong, J. L. M. Rupp, *Adv. Energy Mater.* **2021**, *11*, 2002689.
- [11] Y. Li, Z. Gao, F. Hu, X. Lin, Y. Wei, J. Peng, J. Yang, Z. Li, Y. Huang, H. Ding, *Small Methods* **2020**, *4*, 2000111.
- [12] S. P. Culver, R. Koerver, W. G. Zeier, J. Janek, *Adv. Energy Mater.* **2019**, *9*, 1900626.
- [13] K. Takada, N. Ohta, L. Zhang, K. Fukuda, I. Sakaguchi, R. Ma, M. Osada, T. Sasaki, *Solid State Ionics* **2008**, *179*, 1333–1337.
- [14] F. Walther, F. Strauss, X. Wu, B. Mogwitz, J. Hertle, J. Sann, M. Rohnke, T. Brezesinski, J. Janek, *Chem. Mater.* **2021**, *33*, 2110–2125.
- [15] A.-Y. Kim, F. Strauss, T. Bartsch, J. H. Teo, T. Hatsukade, A. Mazilkin, J. Janek, P. Hartmann, T. Brezesinski, *Chem. Mater.* **2019**, *31*, 9664–9672.
- [16] D. Kitsche, Y. Tang, Y. Ma, D. Goonetilleke, J. Sann, F. Walther, M. Bianchini, J. Janek, T. Brezesinski, *ACS Appl. Energy Mater.* **2021**, *4*, 7338–7345.
- [17] Y. Ito, Y. Sakurai, S. Yubuchi, A. Sakuda, A. Hayashi, M. Tatsumisago, *J. Electrochem. Soc.* **2015**, *162*, A1610–A1616.
- [18] H. Visbal, Y. Aihara, S. Ito, T. Watanabe, Y. Park, S. Doo, *J. Power Sources* **2016**, *314*, 85–92.
- [19] P. Heitjans, M. Masoud, A. Feldhoff, M. Wilkening, *Faraday Discuss.* **2007**, *134*, 67–82.
- [20] V. V. Konovalova, V. V. Fomichev, D. V. Drobot, R. M. Zakalyukin, S. Yu. Stefanovich, *Russ. J. Inorg. Chem.* **2009**, *54*, 1650–1654.
- [21] Y. Li, M. P. Paranthaman, L. W. Gill, E. W. Hagaman, Y. Wang, A. P. Sokolov, S. Dai, C. Ma, M. Chi, G. M. Veith, A. Manthiram, J. B. Goodenough, *J. Mater. Sci.* **2016**, *51*, 854–860.
- [22] F. Strauss, J. H. Teo, J. Maibach, A.-Y. Kim, A. Mazilkin, J. Janek, T. Brezesinski, *ACS Appl. Mater. Interfaces* **2020**, *12*, 57146–57154.
- [23] Y. Ma, J. H. Teo, D. Kitsche, T. Diemant, F. Strauss, Y. Ma, D. Goonetilleke, J. Janek, M. Bianchini, T. Brezesinski, *ACS Energy Lett.* **2021**, *6*, 3020–3028.
- [24] S. H. Jung, K. Oh, Y. J. Nam, D. Y. Oh, P. Brüner, K. Kang, Y. S. Jung, *Chem. Mater.* **2018**, *30*, 8190–8200.
- [25] J.-C. Grenier, C. Martin, A. Durif, *Bull. Soc. Fr. Mineral. Cristallogr.* **1964**, *87*, 316–320.
- [26] D. R. Modeshia, R. I. Walton, M. R. Mitchell, S. E. Ashbrook, *Dalton Trans.* **2010**, *39*, 6031–6036.
- [27] Y.-J. Hsiao, T.-H. Fang, S.-J. Lin, J.-M. Shieh, L.-W. Ji, *J. Lumin.* **2010**, *130*, 1863–1865.
- [28] A.-Y. Kim, F. Strauss, T. Bartsch, J. H. Teo, J. Janek, T. Brezesinski, *Sci. Rep.* **2021**, *11*, 5367.
- [29] F. Xin, H. Zhou, Y. Zong, M. Zuba, Y. Chen, N. A. Chernova, J. Bai, B. Pei, A. Goel, J. Rana, F. Wang, K. An, L. F. J. Piper, G. Zhou, M. S. Whittingham, *ACS Energy Lett.* **2021**, *6*, 1377–1382.
- [30] F. Xin, H. Zhou, J. Bai, F. Wang, M. S. Whittingham, *J. Phys. Chem. Lett.* **2021**, *12*, 7908–7913.
- [31] R. J. Clément, Z. Lun, G. Ceder, *Energy Environ. Sci.* **2020**, *13*, 345–373.
- [32] N. Yabuuchi, M. Takeuchi, M. Nakayama, H. Shiiba, M. Ogawa, K. Nakayama, T. Ohta, D. Endo, T. Ozaki, T. Inamasu, K. Sato, S. Komaba, *Proc. Natl. Acad. Sci. USA* **2015**, *112*, 7650–7655.
- [33] S.-K. Jung, H. Gwon, S.-S. Lee, H. Kim, J. C. Lee, J. G. Chung, S. Y. Park, Y. Aihara, D. Im, *J. Mater. Chem. A* **2019**, *7*, 22967–22976.
- [34] J. H. Teo, F. Strauss, F. Walther, Y. Ma, S. Payandeh, T. Scherer, M. Bianchini, J. Janek, T. Brezesinski, *Mater. Futures* **2022**, *1*, 015102.
- [35] B. H. Toby, R. B. Von Dreele, *J. Appl. Crystallogr.* **2013**, *46*, 544–549.
- [36] L. de Biasi, G. Lieser, J. Rana, S. Indris, C. Dräger, S. Glatthaar, R. Möning, H. Ehrenberg, G. Schumacher, J. R. Binder, H. Geßwein, *CrystEngComm* **2015**, *17*, 6163–6174.
- [37] P. J. Chupas, K. W. Chapman, C. Kurtz, J. C. Hanson, P. L. Lee, C. P. Grey, *J. Appl. Crystallogr.* **2008**, *41*, 822–824.
- [38] G. W. Stinton, J. S. O. Evans, *J. Appl. Crystallogr.* **2007**, *40*, 87–95.

Manuscript received: December 15, 2021  
Revised manuscript received: February 26, 2022  
Version of record online: March 21, 2022